NANO LETTERS

pubs.acs.org/NanoLett Letter

Visualizing Elastocapillary Expansion of Graphene through Bulge Tests

Zhida Gao, Wanying Zheng, Xinjie Liu, Zepu Kou, Zixi Liu, Xiao Wang, Yuyang Long, Chuanli Yu, Baowen Li, Jidong Li, Xuemei Li, Ruixi Qiao, Xiaofei Liu, Lifeng Wang, Zhaohe Dai,* and Jun Yin*

Cite This: https://doi.org/10.1021/acs.nanolett.5c05824 Read Online

ACCESS | Metrics & More | Article Recommendations | Supporting Information

ABSTRACT: The expansion or shrinkage of elastic membranes when wetted by liquids has long been a theoretical concept, yet remained untested due to the extremely small in-plane deformations involved. Here, we leverage out-of-plane bulging to verify that water wetting can indeed cause graphene bubbles to expand. Notably, we find that the graphene bubble becomes "softer" when in contact with water. By incorporating surface tension into Vlassak's model, we obtain a revised equation that accurately attributes the expansion of graphene to the reduction of surface tension at the graphene–water interface. Furthermore, we exploit the underlying principle to actively program deformation and vibrational dynamics of graphene membranes by applying an electric field at the solid–liquid interface. Our results provide fundamental mechanistic insights into the crucial role of surface tension for elastic membranes and open up new avenues for designing responsive structures driven by surface tension.

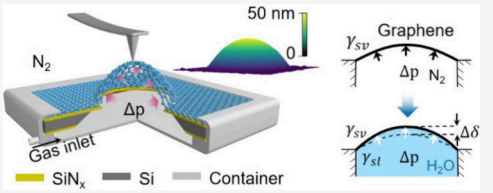

KEYWORDS: *surface tension, graphene bubble, elastocapillary expansion, elastocapillarity, elasto-electro-capillarity*

When a liquid droplet contacts a solid substrate, it deforms to minimize the total surface energies of the system (Figure 1a). This phenomenon, known as wetting, is primarily governed by surface tension.[1,2] Elastic solids are also subject to surface tension, which can influence their deformation, a phenomenon known as elastocapillarity.[3−5] Besides common phenomena of capillary bending, experimental observations on elastocapillarity have mainly been achieved in gel-like ultrasoft solids so far.[3−5] For example, it has been found impossible to fabricate gel slabs with sharp corners, as they are dramatically rounded by the elastocapillary effect.[3] By contrast, the long-theorized expansion or contraction of an elastic membrane upon immersion in a liquid (Figure 1b),[3,6] has remained experimentally elusive. The key challenge lies in that the liquid-induced in-plane strain is extremely small, typically much lower than 10^{-3}, even for ultrasoft gels[3] and atomically thin materials (Supplementary Note 1).

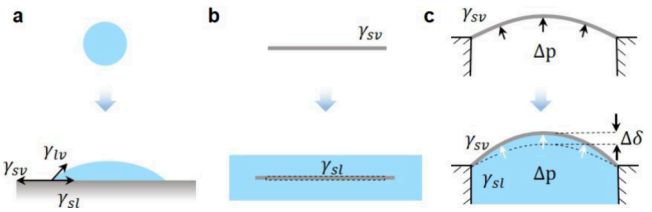

Figure 1. Schematic illustration of the elastocapillarity in an elastic membrane. (a) The spreading of a liquid droplet as it encounters a solid surface. (b) The lateral expansion of a solid disk as it is immersed in a favored liquid. (c) The growth of bubble deflection as the elastic membrane is wetted by a favored liquid.

Although the physical picture in Figure 1b is canonical, surface energy is rarely incorporated into the force balance when analyzing the deformation of elastic membranes under external loading.[6] In the limiting case of a soap membrane with zero elasticity, it is well-established that the external load has to deal with surface tension.[7] However, even for 2D elastic membranes with atomic thinness, the literature at large overlooks their surface tension.[8−11] Consequently, the influence of surface tension or, more broadly, solid–liquid interactions, on the mechanical response of 2D materials remains largely unquantified. Clarifying this contribution is essential for understanding elastocapillary effects in 2D materials and may inform the design of surface-tension-driven actuators, sensors, and tunable nanomechanical systems.

In this work, we experimentally clarify the role of surface tension in the mechanical behavior of 2D materials by investigating their elastocapillary expansion, typically in graphene. Rather than examining the ultralow in-plane deformation, we clamp the graphene edges and monitor its out-of-plane elastocapillary response (Figure 1c), which can be facilely detected through well-established techniques, including

Received: November 22, 2025
Revised: January 7, 2026
Accepted: January 12, 2026

atomic force microscopy (AFM)[9,12−14] and optical interference.[15,16] Our findings reveal that the surface tension is, in fact, pivotal to the mechanical behavior of elastic membranes. Additionally, we demonstrate that the deflection of graphene bubbles can be effectively modified by applying an electric field across the solid−liquid interface, which essentially makes use of elasto-electro-capillarity.

The experimental setup is schematically illustrated in Figure 2a. Suspended graphene membranes were fabricated by transferring mechanically exfoliated monolayer graphene flakes, which were free of defects and grain boundaries (Figure S1), over a predefined SiN_x aperture (diameter ∼3 μm, unless otherwise stated).[17] Details are provided in Methods and Supplementary Note 2. The resulting device was then clamped onto a compact container (Figure 2b), whose internal pressure was adjusted in situ using pressurized nitrogen gas (N_2) delivered through a mass-flow meter and monitored by a pressure gauge (Figure S2a). The pressure difference (Δp) across the suspended graphene membrane causes it to bulge upward (inset of Figure 2a), and the bubble topography at various Δp was measured by AFM (Figure S2b). Although monolayer graphene can partially transmit electrostatic potentials from the underlying medium[18] and could, in principle, influence the effective tip−sample interaction,[19] AFM pull-off adhesion tests (Supplementary Note 4) indicate that water beneath graphene does not contribut a measurable change in the effective tip−graphene interaction under our experimental conditions, mainly due to the much small dielectric response of water as revealed by Lifshitz theory calculations (Supplementary Note 4). Because the maximum bubble deflection (δ) far exceeded the graphene thickness (t) (ratio ∼24−188), bending rigidity could be neglected,[9,14,20] as further verified numerically (Supplementary Note 9). The deflection profiles were therefore well described by membrane theory (Figure 2c, Supplementary Note 5),[21] parametrized by its δ and radius, R.

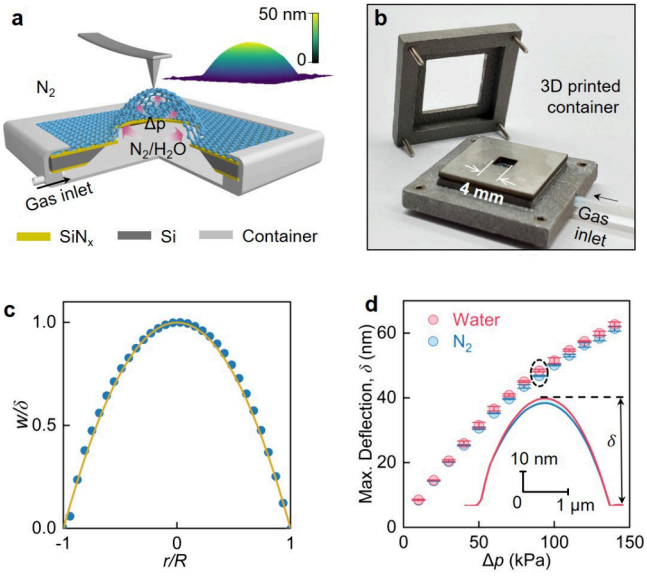

Figure 2. Device setup and characterization of graphene bubble. (a) Schematic of the experimental setup. The internal surface of the graphene bubble interfaces with N_2 or water. The inset illustrates a typical three-dimensional topography of a graphene bubble. (b) Optical image of the container. The cover and base were fastened with four screws after loading the device, with a polydimethylsiloxane (PDMS) film and an O-ring sealing the upper and lower interfaces between the container and the device. (c) Normalized deflection profile of a graphene bubble. The orange curve shows a membrane-theory fit neglecting bending stiffness. w and r denote the out-of-plane deflection and radial position, respectively. (d) The δ versus Δp for a graphene bubble interfacing with N_2 (blue markers) and water (red markers), respectively. The error bars represent the standard deviation of δ extracted from a single device over multiple (more than three times) loading−unloading cycles under identical interfacial conditions (either N_2 or water). The inset illustrates the deflection profiles of the bubble crossing its center measured at 90 kPa, where δ_{N_2} = 46.78 ± 0.14 nm, δ_{water} = 48.45 ± 0.40 nm, yielding an average difference of $\Delta\delta$ = 1.67 nm.

Wetting-induced deformation was investigated by comparing deflection of pressurized graphene bubbles interfacing with N_2 and water. Bulk water was placed on the bottom surface of the graphene membrane, instead of its top surface, to prevent changes in the damping properties of the AFM cantilever during top-surface imaging, which could lead to discrepancies in the measured topography.[22] The direct contact between the water and graphene without trapped gas at the interface was confirmed by Raman mapping (Figure S6, Supplementary Note 6), evidenced by the uniformity in both the blue shift of graphene Raman peaks and the intensity of water-related Raman signals[23] over the whole suspended area. Additionally, only wrinkle-free graphene membranes were selected for testing and mechanical analysis (Figure S7).

During bulge testing, the graphene bubble was subjected to pressure cycles from 10 to 140 kPa in 10 kPa increments, repeated three times. The gas/liquid interface introduced a small pressure offset in water-contact tests, but this deviation (<72 Pa) was negligible due to its orders of magnitude lower than the lowest applied pressure (Supplementary Note 3). The δ was highly reversible and remained nearly consistent at each Δp throughout the cyclic tests (Figure S8a). Notably, the wetting-induced changes in both Raman spectra (Figure S6a) and deflection profiles (Figure S8b) were also fully reversible, indicating no plastic deformation, fracture, lattice defects, sliding, or delamination at the graphene-SiN_x interface. The stability of the graphene membrane and its secure clamping to the SiN_x substrate ensure the reliability of our measurements.

The dependence of δ on Δp of a representative device, which is applied by pressurizing N_2 and water, is presented in Figure 2d. Intriguingly, deflection of the graphene bubble in contact with water was consistently higher than that with N_2 at varied pressure levels. This is a signature of the surface tension effect as illustrated by the elastocapillary expansion of graphene in Figure 1. We note that if examining the expansion of graphene of stretching stiffness E_{2D} due to surface tension γ in an in-plane way, the corresponding deformation ratio scales as γ/E_{2D}, and hence the corresponding displacement for a micron-sized graphene $\gamma R/E_{2D}$ is on the order of only 0.1 nm (Supplementary Note 1). This exceeds the capabilities of state-of-the-art displacement measurement technology applicable to such systems.[24] In contrast, at Δp = 90 kPa, for example, the corresponding change in graphene deflection reaches 1.67 nm, highlighting the advantage of the out-of-plane bulging method for clarifying the elastocapillary effect on graphene membranes.

To rationalize the observed elastocapillary expansion of graphene, we revise Vlassak's expression by considering the effect of surface tension.[25] The mechanical schematic of the bubble is shown in Figure 3a. The small aspect ratio (δ/R, less

https://doi.org/10.1021/acs.nanolett.5c05824
Nano Lett. XXXX, XXX, XXX−XXX

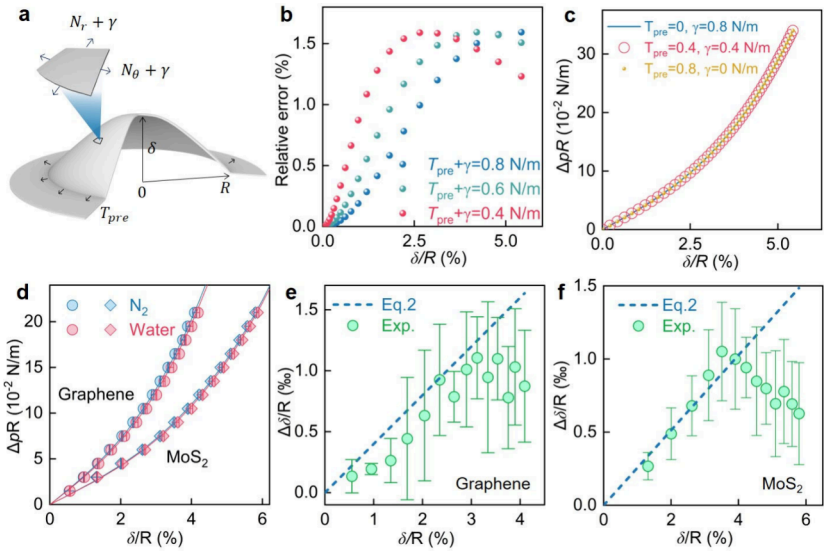

Figure 3. Mechanism of elastocapillary expansion in pressurized graphene and MoS_2 bubbles. (a) Schematic of a pressurized bubble. The inset illustrates the radial (N_r) and hoop (N_θ) elastic tensions, along with the surface tension acting on a representative element. (b) Relative error between numerical and analytical results for three different total tensions ($T_{pre} + \gamma$). (c) ΔpR versus the calculated δ/R for different pretension/surface tension conbinations. (d) ΔpR versus the measured δ/R for graphene and MoS_2 bubbles. Solid lines are fits to eq 1. Error bars represent the standard deviation of bubble deflection measurements across three dry-wet cycles. (e and f) Wetting-induced change in deflection $\Delta\delta/R$ plotted against the normalized dry deflection δ/R for graphene (e) and MoS_2 (f) bubbles. Dashed lines show the theoretical prediction from eq 2. Error bars denote the standard deviation of the deflection differences obtained in each dry-wet cycle.

than 0.1) of the graphene bubble and the absence of slip at the graphene−substrate interface (Figure S8, Supplementary Note 7) allow the graphene to be modeled as a circular, linearly elastic membrane with a clamped boundary,[20] and the graphene-substrate interface energy does not play in practice. The surface energy is incorporated by integrating the surface energy density (γ) over the deformed area. Since the maximum stretching strain is below 1‰ (Figure S9a, Supplementary Note 8), the strain dependence of γ can be neglected.[25] Consequently, surface tension equals the surface energy density: $\gamma = \gamma_{sv} + \gamma_{sl}$ for the water-graphene-vapor interface and $\gamma = 2\gamma_{sv}$ for the vapor-graphene-vapor interface.

Combining variational analysis and numerical verification (Supplementary Note 9), we find the mechanical response of graphene to applied pressure, considering the surface tension, is well approximated by

$$\Delta pR = 4(T_{pre} + \gamma)\frac{\delta}{R} + \alpha E_{2D}\left(\frac{\delta}{R}\right)^3 \quad (1)$$

where T_{pre} is the fabrication-induced pretension, and α is a constant depending on Poisson's ratio ($\alpha \approx 3.10$ for graphene[8]). The linear and cubic terms in eq 1 characterize the small and large deflection regimes, respectively. Unlike a soap bubble, which resists pressure solely through surface tension,[7] the graphene bubble resists pressure through a combination of pretension, surface tension, and intrinsic elasticity. The relative error between numerical results and eq 1 is found within 2%, indicating the accuracy of our analytical model (Figure 3b). Furthermore, $\Delta p-\delta$ curves computed for three different combinations of pretension and surface tension (Figure 3c), but with identical total tension ($T_{pre} + \gamma$), collapse onto a single curve, indicating that surface tension acts analogously to pretension as both follow the Laplace law.

Figure 3d shows the plot of ΔpR versus the measured δ/R. The experimental data agree well with eq 1, as indicated by the solid fitting curves. The stretching modulus of graphene for this specimen is determined to be 389 ± 2.9 N/m, consistent with the previously reported values.[26,27] For graphene in N_2, $T_{pre} + \gamma$ is 0.781 ± 0.003 N/m, which decreases to 0.751 ± 0.003 N/m when the internal surface contacts water. Notably, the reversible bulging response confirms that T_{pre} remains constant during the test, implying that γ decreases by around 30 mN/m upon wetting.

To assess the reproducibility of the observed elastocapillary expansion, we performed the same analysis on another suspended graphene device (Supplementary Note 10). The extracted $\Delta\gamma$ values are 26 mN/m, giving $\Delta\gamma = 28 \pm 2.83$ mN/m as an estimate of sample-to-sample variability. This reduction corresponds to $\Delta\gamma = \gamma_{sv} - \gamma_{sl}$, and agrees with earlier measurements obtained from surface forces apparatus studies on supported graphene[28] and graphene wettability measurements.[29] Generally, the elastocapillary expansion can be explained as a reduction in the work needed to increase the interfacial area in the graphene−water system. Therefore, relatively smaller external work (or pressure) is required to produce graphene bubbles of the same height using water than using N_2. We note that unlike prior studies on freely floating thin sheets,[6] our clamped-membrane configuration allows direct quantification of $\Delta\gamma$ through out-of-plane bulging.

We have revealed the important role of surface tension in controlling the mechanical behavior of graphene membranes. Such a role, however, has been generally overlooked in both in-plane and out-of-plane experiments involving 2D materials and various other nanofilms.[6,8−11] Equation 1 may give some hints as to why this oversight has not posed significant issues: surface tension and pretension effects are intertwined. Taking the surface energy of graphite (from 0.14 to 0.34 J/m^2) as a reference,[30−32] our samples exhibit T_{pre} in the range between 0.1 and 0.5 N/m,[26] comparable to γ. Consequently, the

https://doi.org/10.1021/acs.nanolett.5c05824
Nano Lett. XXXX, XXX, XXX−XXX

pretension has obscured the clarification of the elastocapillary effects in elastic membranes. The key to our finding is the controlled experiments in which the surface tension changes while the pretension remains constant.

We further demonstrate that the elastocapillary expansion of graphene can be amplified by the increasing deflection. According to eq 1, the increase in deflection induced by water wetting under a fixed pressure is (Supplementary Note 9)

$$\frac{\Delta\delta}{R} = \frac{\Delta\gamma}{T_{pre} + \gamma_{sv} + \gamma_{sl}} \times \frac{\delta}{R} \tag{2}$$

at small deflections, i.e. when $\delta/R \leq ((T_{pre} + \gamma)/E_{2D})^{1/2} \sim 4\%$. Figure 3e plots $\Delta\delta/R$ versus δ/R, showing an initial linear increase consistent with eq 2. At larger deflections ($\delta/R > 4\%$), the stretching effect of the graphene membrane becomes dominant, diminishing the influence of both pretension and surface tension and causing $\Delta\delta$ to decrease with applied pressure. To further validate the generality of our findings, we applied identical bulge tests on monolayer MoS_2 membranes (Figure S10). As shown in Figure 3f, MoS_2 exhibits similar elastocapillary expansion accurately captured by eq 2, confirming that the observed elastocapillary behavior is applicable to other 2D materials.

Although previously overlooked, the elastocapillary expansion we verified provides valuable opportunities for controlling the mechanical behavior of elastic membranes. To demonstrate this, we tune γ_{sl} through applying an electric field at the solid−liquid interface, thereby modifying the graphene deflection. At the graphene-electrolyte interface, an electric double layer (EDL) forms spontaneously and functions as a parallel plate capacitor, storing electrostatic energy. This stored energy reduces the solid−liquid interfacial energy[33] and the voltage-dependent change in interfacial energy is given by[34]

$$\Delta\gamma_{sl}(V) = \frac{c}{2}(V^2 - 2VV_{pzc}) \tag{3}$$

where c is the EDL capacitance density, V is the applied voltage, and V_{pzc} is the potential of zero charge. For $V \ll V_{pzc}$, eq 3 simplifies to $\Delta\gamma_{sl}(V) \approx -cVV_{pzc}$. Thus, under small pressure levels, the electric modulation of deflection can be approximated by

$$\Delta\delta = \frac{-\delta c V_{pzc}}{T_{pre} + \gamma_{sv} + \gamma_{sl} - \Delta\gamma_{sl}(V)} \times V \tag{4}$$

To experimentally verify the elastoelectrocapillary effect, we used 0.1 M KCl as the electrolyte, for which the V_{pzc} of suspended monolayer graphene on 0.1 M KCl solution has been specifically determined to be ∼ 0.5 V.[35] The applied voltage was limited to tens of millivolts to satisfy $V \ll V_{pzc}$ and to avoid the interlayer intercalation near 0.1 V.[36]

As shown in Figure 4b, the variation in bubble deflection under a direct-current (DC) voltage was measured by AFM. The bubble radius is around 2.2 μm. Fitting the $\Delta p - \delta$ (measured in N_2 condition) data with eq 1 yields a $T_{pre}+2\gamma_{sv}$ around 0.400 ± 0.003 N/m (Figure 4a). While wetted by water at Δp = 30 kPa, the maximum bubble deflection increases from 73 to 78.5 nm (Figure 4c), corresponding to $T_{pre}+\gamma_{sv} + \gamma_{sl} \approx 0.374$ N/m. As shown in Figure 4c, under a constant Δp, the deflection increases monotonically as the applied bias decreases from 50 to −50 mV, and the response is fully reversible across three test cycles, returning to 78.5 nm after removing the voltage. The experimental results closely match the predictions of eq 4, as indicated by the dotted line. An EDL thickness of 1 nm was used in the calculation, a reasonable value for a 0.1 M KCl solution.[37]

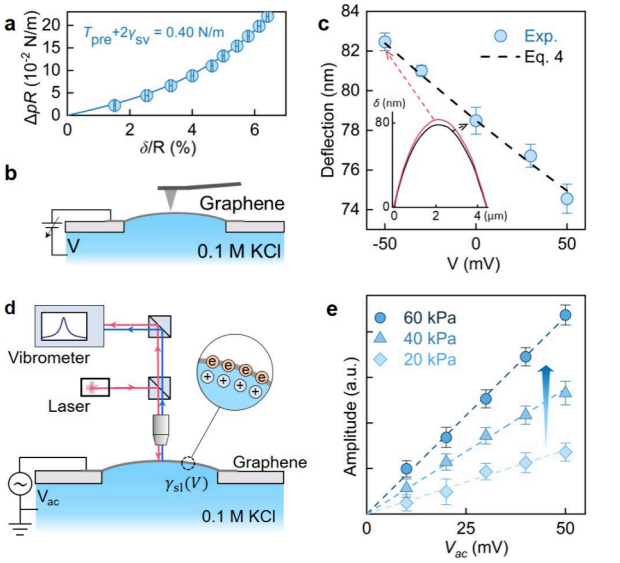

Figure 4. Elasto-electro-capillarity of graphene. (a) ΔpR versus the measured δ/R in N_2. Solid lines are fits to eq 1. (b) Schematic for elastoelectrocapillary actuation under DC voltage. (c) Dependence of δ on the applied direct-current voltage ranging from −50 to 50 mV. The dotted line represents the prediction of eq 4. The inset compares the deflection profiles crossing bubble center at 0 mV (black) and −50 mV (red). (d) Schematic illustration of the setup for detecting graphene vibration. The inset schematically illustrates the EDL of the graphene-solution interface. (e) Vibration amplitude of the graphene membrane as a function of V_{ac} at varied Δp. Dashed lines represent fits to eq 4.

Motivated by our static electromechanical characterization under DC bias, we further examined the dynamic excitation of graphene bubbles by applying an alternating voltage V_{ac} between graphene and water. As shown in Figure 4d, the resulting out-of-plane motion was detected optically via interferometry.[15,16] Figure 4e shows the vibrational amplitude versus V_{ac} for a graphene membrane supported over a SiN_x aperture with a radius of 2.2 μm. Because membrane vibration at a liquid interface is influenced by liquid viscosity, hydrodynamic loading, and interfacial shear stresses, a purely quasi-static model is not enough to capture the vibration amplitude quantitatively. Nevertheless, the amplitude increases monotonically with V_{ac}, qualitatively consistent with the trend predicted by the eq 4. Notably, the positive correlation between pressure difference and vibration amplitude distinguishes the excitation mechanism of our device from traditional electromechanical resonators driven by electrostatic force, in which the vibration amplitude typically decreases with increased membrane tension.[38]

By interfacing graphene with N_2 and water, we experimentally verify elastocapillary expansion in 2D elastic membranes through out-of-plane bulging. The results showed that solid−liquid interactions are crucial to the mechanical response of elastic membranes to external forces, particularly at the onset of external loading. Building on this insight, we have demonstrated that alterations in surface tension, triggered by electrocapillary wetting, can modify the deflection of graphene bubbles. We anticipate exciting applications and novel

https://doi.org/10.1021/acs.nanolett.5c05824
Nano Lett. XXXX, XXX, XXX−XXX

responsive structures inspired by this interplay between wetting and mechanical response. For instance, integrating a graphene/water microlens into an optical platform would allow electrical tuning of bubble deflection and thereby tune the focal length of the microlens.

METHODS

Device Fabrication

A free-standing silicon nitride (SiN_x) window on a silicon cavity was prepared through anisotropic etching of (100) silicon wafers, with both sides coated with 500 nm of SiN_x.[17] A circular hole was drilled into the SiN_x window using reactive ion etching with a prepatterned photoresist mark. Mechanically exfoliated monolayer graphene was transferred onto the aperture via a poly(methyl methacrylate) (PMMA)-assisted dry transfer technique,[39] after which the PMMA was removed with acetone and the sample was supercritically dried to minimize membrane sagging. The layer number and quality of the targeted graphene flakes were verified by Raman spectroscopy prior to transfer[23] (Figure S6). To investigate the elastocapillary expansion, water was introduced into the silicon cavity, and any entrapped air was removed by placing the device in a chamber 80 kPa below ambient for 10 min.

AFM Measurements of the Pressurized Bubbles

The topography of bubbles was imaged by an AFM (SPI3800N, SII Nanotechnology Inc.) operated in tapping mode to minimize tip−sample shearing force and avoid bubble distortion.[40] The cantilever had a nominal spring constant of ∼9 N/m, a resonance frequency ∼160 kHz, and a free oscillation amplitude of ∼85 nm. The set point ratio was 0.8. the nominal tip radius was ∼10 nm, and the scan rate was 0.5 Hz. All measurements were performed in a dry environment with blowing N_2.

Optical Characterization of the Elastoelectrocapillarity

For dynamic excitation, a radio frequency voltage (1.6 MHz) between graphene and the silicon wafer in contact with water. The out-of-plane motion of the graphene bubble was detected by monitoring the reflected light superimposed with a reference beam through a laser Doppler vibrometer system (MSA-100-3D, Polytec). Tests were conducted using a 633 nm laser spot with a diameter of approximately 4 μm in ambient.

ASSOCIATED CONTENT

Supporting Information

The Supporting Information is available free of charge at https://pubs.acs.org/doi/10.1021/acs.nanolett.5c05824.

Detailed device fabrication and additional experimental results (PDF)

AUTHOR INFORMATION

Corresponding Authors

Zhaohe Dai − *School of Mechanics and Engineering Science, State Key Laboratory for Turbulence and Complex Systems, Peking University, Beijing 100871, China;* orcid.org/0000-0002-5205-089X; Email: daizh@pku.edu.cn

Jun Yin − *State Key Laboratory of Mechanics and Control of Mechanical Structures, Key Laboratory for Intelligent Nano Materials and Devices of the Ministry of Education and College of Aerospace Engineering, Nanjing University of Aeronautics and Astronautics, Nanjing 210016, P. R. China;* Email: yinjun@nuaa.edu.cn

Authors

Zhida Gao − *State Key Laboratory of Mechanics and Control of Mechanical Structures, Key Laboratory for Intelligent Nano Materials and Devices of the Ministry of Education and College of Aerospace Engineering, Nanjing University of Aeronautics and Astronautics, Nanjing 210016, P. R. China*

Wanying Zheng − *School of Mechanics and Engineering Science, State Key Laboratory for Turbulence and Complex Systems, Peking University, Beijing 100871, China*

Xinjie Liu − *College of Aerospace Engineering, Nanjing University of Aeronautics and Astronautics, Nanjing 210016, P. R. China;* orcid.org/0000-0002-2619-1963

Zepu Kou − *State Key Laboratory of Mechanics and Control of Mechanical Structures, Key Laboratory for Intelligent Nano Materials and Devices of the Ministry of Education and College of Aerospace Engineering, Nanjing University of Aeronautics and Astronautics, Nanjing 210016, P. R. China*

Zixi Liu − *Institute for Frontier Science, Nanjing University of Aeronautics and Astronautics, Nanjing 210016, P. R. China*

Xiao Wang − *State Key Laboratory of Mechanics and Control of Mechanical Structures, Key Laboratory for Intelligent Nano Materials and Devices of the Ministry of Education and College of Aerospace Engineering, Nanjing University of Aeronautics and Astronautics, Nanjing 210016, P. R. China*

Yuyang Long − *State Key Laboratory of Mechanics and Control of Mechanical Structures, Key Laboratory for Intelligent Nano Materials and Devices of the Ministry of Education and College of Aerospace Engineering, Nanjing University of Aeronautics and Astronautics, Nanjing 210016, P. R. China*

Chuanli Yu − *School of Mechanics and Engineering Science, State Key Laboratory for Turbulence and Complex Systems, Peking University, Beijing 100871, China;* orcid.org/0000-0001-8480-5591

Baowen Li − *State Key Laboratory of Mechanics and Control of Mechanical Structures, Key Laboratory for Intelligent Nano Materials and Devices of the Ministry of Education and College of Aerospace Engineering, Nanjing University of Aeronautics and Astronautics, Nanjing 210016, P. R. China*

Jidong Li − *Institute for Frontier Science, Nanjing University of Aeronautics and Astronautics, Nanjing 210016, P. R. China*

Xuemei Li − *College of Material Science and Engineering, Nanjing University of Aeronautics and Astronautics, Nanjing 210016, P. R. China*

Ruixi Qiao − *Institute for Frontier Science, Nanjing University of Aeronautics and Astronautics, Nanjing 210016, P. R. China*

Xiaofei Liu − *State Key Laboratory of Mechanics and Control of Mechanical Structures, Key Laboratory for Intelligent Nano Materials and Devices of the Ministry of Education and College of Aerospace Engineering, Nanjing University of Aeronautics and Astronautics, Nanjing 210016, P. R. China;* orcid.org/0000-0003-0563-3600

Lifeng Wang − *College of Aerospace Engineering, Nanjing University of Aeronautics and Astronautics, Nanjing 210016, P. R. China;* orcid.org/0000-0001-9563-8282

Complete contact information is available at: https://pubs.acs.org/10.1021/acs.nanolett.5c05824

Author Contributions

Z. Gao and W. Zheng contributed equally. J. Yin conceived the project. Z. Gao performed the experiments with assistance from X. Liu, X. Wang, Y. Long, C. Yu, and B. Li. W. Zheng performed the theoretical studies under the supervision of Z. Dai. The optical interferometry measurement was completed

https://doi.org/10.1021/acs.nanolett.5c05824
Nano Lett. XXXX, XXX, XXX−XXX

under the assistance of X. Liu and the supervision of L. Wang. Z. Kou performed the Lifshitz-theory calculations of the tip−graphene interaction under the guidance of X. Liu. Z. Liu performed high resolution TEM measurement under the supervision of R. Qiao. Z. Gao, W. Zheng, Z. Dai, and J. Yin wrote the paper. All authors contributed to the general discussion and preparation of the manuscript.

Notes

The authors declare no competing financial interest.

■ ACKNOWLEDGMENTS

This work was supported by the National Key Research and Development Program of China (2024YFA1409600), National Natural Science Foundation of China (T2293691, T2293692, 12302133, 12272181, 12372103), Scientific Research Innovation Capability Support Project for Young Faculty (SRICSPYF-ZY2025057), Natural Science Foundation of Jiangsu Province (BK20253057, BK20243065, BK20230875), Fundamental and Interdisciplinary Disciplines Breakthrough Plan of the Ministry of Education of China (JYB2025XDXM205), the Research Fund of State Key Laboratory of Mechanics and Control for Aerospace Structures (MCAS-I-0125Y01, MCAS-I-0124G04, MCAS-I-0525K01), the Fundamental Research Funds for the Central Universities (NE2023003, NJ2024001) and the Fund of Prospective Layout of Scientific Research for NUAA (Nanjing University of Aeronautics and Astronautics).

■ REFERENCES

(1) Fan, J.; De Coninck, J.; Wu, H.; Wang, F. Microscopic Origin of Capillary Force Balance at Contact Line. *Phys. Rev. Lett.* **2020**, *124* (12), No. 125502.
(2) Bonn, D.; Eggers, J.; Indekeu, J.; Meunier, J.; Rolley, E. Wetting and Spreading. *Rev. Mod. Phys.* **2009**, *81* (2), 739−805.
(3) Bico, J.; Reyssat, É.; Roman, B. Elastocapillarity: When Surface Tension Deforms Elastic Solids. *Annu. Rev. Fluid Mech.* **2018**, *50* (1), 629−659.
(4) Schroll, R. D.; Adda-Bedia, M.; Cerda, E.; Huang, J.; Menon, N.; Russell, T. P.; Toga, K. B.; Vella, D.; Davidovitch, B. Capillary Deformations of Bendable Films. *Phys. Rev. Lett.* **2013**, *111* (1), No. 014301.
(5) Singh, K.; Lister, J. R.; Vella, D. A Fluid-Mechanical Model of Elastocapillary Coalescence. *J. Fluid Mech.* **2014**, *745*, 621−646.
(6) Kumar, D.; Russell, T. P.; Davidovitch, B.; Menon, N. Stresses in Thin Sheets at Fluid Interfaces. *Nat. Mater.* **2020**, *19* (7), 690−693.
(7) Pisano, A. *Bubbles, Tracheal Tube Cuffs, and Reservoir Bags: Surface Tension and Laplace's Law*; Springer International Publishing: 2021; pp 61−74.
(8) Dai, Z.; Lu, N. Poking and Bulging of Suspended Thin Sheets: Slippage, Instabilities, and Metrology. *Journal of the Mechanics and Physics of Solids* **2021**, *149*, No. 104320.
(9) Wang, G.; Dai, Z.; Wang, Y.; Tan, P.; Liu, L.; Xu, Z.; Wei, Y.; Huang, R.; Zhang, Z. Measuring Interlayer Shear Stress in Bilayer Graphene. *Phys. Rev. Lett.* **2017**, *119* (3), No. 036101.
(10) Wang, Y.; Feng, S.; Peng, D.; Li, T.; Zheng, C.; Cai, Z.; Wu, Z.; Zheng, Q.; Xu, Z. Intrinsic Interlayer Shear Strength of Graphite. *Journal of the Mechanics and Physics of Solids* **2024**, *193*, No. 105853.
(11) Wang, G.; Zhang, Z.; Wang, Y.; Gao, E.; Jia, X.; Dai, Z.; Weng, C.; Liu, L.; Zhang, Y.; Zhang, Z. Out-of-Plane Deformations Determined Mechanics of Vanadium Disulfide (VS_2) Sheets. *ACS Appl. Mater. Interfaces* **2021**, *13* (2), 3040−3050.
(12) Cui, X.; Liu, L.; Dong, W.; Zhou, Y.; Zhang, Z. Mechanics of 2D Material Bubbles. *Nano Research* **2023**, *16* (12), 13434−13449.
(13) Koenig, S. P.; Boddeti, N. G.; Dunn, M. L.; Bunch, J. S. Ultrastrong Adhesion of Graphene Membranes. *Nat. Nanotechnol.* **2011**, *6* (9), 543−546.
(14) Sanchez, D. A.; Dai, Z.; Wang, P.; Cantu-Chavez, A.; Brennan, C. J.; Huang, R.; Lu, N. Mechanics of Spontaneously Formed Nanoblisters Trapped by Transferred 2D Crystals. *Proc. Natl. Acad. Sci. U. S. A.* **2018**, *115* (31), 7884−7889.
(15) Xu, B.; Zhang, P.; Zhu, J.; Liu, Z.; Eichler, A.; Zheng, X.-Q.; Lee, J.; Dash, A.; More, S.; Wu, S.; Wang, Y.; Jia, H.; Naik, A.; Bachtold, A.; Yang, R.; Feng, P. X. L.; Wang, Z. Nanomechanical Resonators: Toward Atomic Scale. *ACS Nano* **2022**, *16* (10), 15545−15585.
(16) Zhu, J.; Xu, B.; Xiao, F.; Liang, Y.; Jiao, C.; Li, J.; Deng, Q.; Wu, S.; Wen, T.; Pei, S.; Xia, J.; Wang, Z. Frequency Scaling, Elastic Transition, and Broad-Range Frequency Tuning in WSe2 Nanomechanical Resonators. *Nano Lett.* **2022**, *22* (13), 5107−5113.
(17) Wang, H.; Su, L.; Yagmurcukardes, M.; Chen, J.; Jiang, Y.; Li, Z.; Quan, A.; Peeters, F. M.; Wang, C.; Geim, A. K.; Hu, S. Blue Energy Conversion from Holey-Graphene-like Membranes with a High Density of Subnanometer Pores. *Nano Lett.* **2020**, *20* (12), 8634−8639.
(18) Kim, Y.; Cruz, S. S.; Lee, K.; Alawode, B. O.; Choi, C.; Song, Y.; Johnson, J. M.; Heidelberger, C.; Kong, W.; Choi, S.; Qiao, K.; Almansouri, I.; Fitzgerald, E. A.; Kong, J.; Kolpak, A. M.; Hwang, J.; Kim, J. Remote Epitaxy Through Graphene Enables Two-Dimensional Material-Based Layer Transfer. *Nature* **2017**, *544* (7650), 340−343.
(19) Yu, J.; Scheibner, C.; Liang, C.; Witten, T. A.; Vitelli, V.; Park, J. Intrinsic Wrinkling of Free-Standing Polycrystalline Atomically Thin Films. *ACS Nano* **2025**, *19* (27), 24831−24840.
(20) Dai, Z.; Hou, Y.; Sanchez, D. A.; Wang, G.; Brennan, C. J.; Zhang, Z.; Liu, L.; Lu, N. Interface-Governed Deformation of Nanobubbles and Nanotents Formed by Two-Dimensional Materials. *Phys. Rev. Lett.* **2018**, *121* (26), No. 266101.
(21) Dai, Z. Analytical Solutions for Circular Elastic Membranes Under Pressure. *Journal of Applied Mechanics* **2024**, *91* (8), No. 081002.
(22) Chen, X.; Li, B.; Liao, Z.; Li, J.; Li, X.; Yin, J.; Guo, W. Principles and Applications of Liquid-Environment Atomic Force Microscopy. *Advanced Materials Interfaces* **2022**, *9* (35), 2201864.
(23) Belyaeva, L. A.; Jiang, L.; Soleimani, A.; Methorst, J.; Risselada, H. J.; Schneider, G. F. Liquids Relax and Unify Strain in Graphene. *Nat. Commun.* **2020**, *11* (1), 898.
(24) Ren, Q.; Liu, J.; Zhu, C.; Qiu, W.; Zhao, J.; Wang, H.; Zhao, P. Interfacial Damage of Bilayer Graphene Under Shear Deformation: Theory, Experiment, and Simulation. *Journal of the Mechanics and Physics of Solids* **2023**, *171*, No. 105154.
(25) Rao, Y.; Qiao, S.; Dai, Z.; Lu, N. Elastic Wetting: Substrate-Supported Droplets Confined by Soft Elastic Membranes. *Journal of the Mechanics and Physics of Solids* **2021**, *151*, No. 104399.
(26) Lee, C.; Wei, X.; Kysar, J. W.; Hone, J. Measurement of the Elastic Properties and Intrinsic Strength of Monolayer Graphene. *Science* **2008**, *321* (5887), 385−388.
(27) Cao, K.; Feng, S.; Han, Y.; Gao, L.; Hue Ly, T.; Xu, Z.; Lu, Y. Elastic Straining of Free-Standing Monolayer Graphene. *Nat. Commun.* **2020**, *11* (1), 284.
(28) van Engers, C. D.; Cousens, N. E. A.; Babenko, V.; Britton, J.; Zappone, B.; Grobert, N.; Perkin, S. Direct Measurement of the Surface Energy of Graphene. *Nano Lett.* **2017**, *17* (6), 3815−3821.
(29) Zhang, J.; Jia, K.; Huang, Y.; Liu, X.; Xu, Q.; Wang, W.; Zhang, R.; Liu, B.; Zheng, L.; Chen, H.; Gao, P.; Meng, S.; Lin, L.; Peng, H.; Liu, Z. Intrinsic Wettability in Pristine Graphene. *Adv. Mater.* **2022**, *34* (6), No. 2103620.
(30) Koren, E.; Lörtscher, E.; Rawlings, C.; Knoll, A. W.; Duerig, U. Adhesion and Friction in Mesoscopic Graphite Contacts. *Science* **2015**, *348* (6235), 679−683.
(31) Liu, Z.; Liu, J. Z.; Cheng, Y.; Li, Z.; Wang, L.; Zheng, Q. Interlayer Binding Energy of Graphite: A Mesoscopic Determination from Deformation. *Phys. Rev. B* **2012**, *85* (20), No. 205418.
(32) Wang, W.; Dai, S.; Li, X.; Yang, J.; Srolovitz, D. J.; Zheng, Q. Measurement of the Cleavage Energy of Graphite. *Nat. Commun.* **2015**, *6* (1), 7853.

https://doi.org/10.1021/acs.nanolett.5c05824
Nano Lett. XXXX, XXX, XXX−XXX

(33) Chakraborty, S. Electrocapillary. In *Encyclopedia of Microfluidics and Nanofluidics*, Li, D., Ed.; Springer US: 2008; pp 460−469.
(34) Mugele, F.; Baret, J.-C. Electrowetting: from Basics to Applications. *J. Phys.: Condens. Matter* **2005**, *17* (28), R705−R774.
(35) Xu, Y.; Ma, Y. B.; Gu, F.; Yang, S. S.; Tian, C. S. Structure Evolution at the Gate-Tunable Suspended Graphene-Water Interface. *Nature* **2023**, *621* (7979), 506−510.
(36) Zhao, J.; Zou, X.; Zhu, Y.; Xu, Y.; Wang, C. Electrochemical Intercalation of Potassium into Graphite. *Adv. Funct. Mater.* **2016**, *26* (44), 8103−8110.
(37) Smith, A. M.; Lee, A. A.; Perkin, S. The Electrostatic Screening Length in Concentrated Electrolytes Increases with Concentration. *J. Phys. Chem. Lett.* **2016**, *7* (12), 2157−2163.
(38) Lee, J.; Wang, Z.; He, K.; Yang, R.; Shan, J.; Feng, P. X.-L. Electrically Tunable Single- and Few-Layer MoS_2 Nanoelectromechanical Systems With Broad Dynamic Range. *Science Advances* **2018**, *4* (3), No. eaao6653.
(39) Tien, D. H.; Park, J. Y.; Kim, K. B.; Lee, N.; Choi, T.; Kim, P.; Taniguchi, T.; Watanabe, K.; Seo, Y. Study of Graphene-based 2D-Heterostructure Device Fabricated by All-Dry Transfer Process. *ACS Appl. Mater. Interfaces* **2016**, *8* (5), 3072−8.
(40) Ares, P.; Wang, Y. B.; Woods, C. R.; Dougherty, J.; Fumagalli, L.; Guinea, F.; Davidovitch, B.; Novoselov, K. S. Van der Waals Interaction Affects Wrinkle Formation in Two-Dimensional Materials. *Proc. Natl. Acad. Sci. U. S. A.* **2021**, *118* (14), No. e2025870118.

https://doi.org/10.1021/acs.nanolett.5c05824
Nano Lett. XXXX, XXX, XXX−XXX